

Interdecadal change of interannual variability and predictability of two types of ENSO

Hye-In Jeong · Joong-Bae Ahn · June-Yi Lee ·
Andrea Alessandri · Harry H. Hendon

Received: 26 September 2013 / Accepted: 26 March 2014 / Published online: 19 April 2014
© Springer-Verlag Berlin Heidelberg 2014

Abstract A significant interdecadal climate shift of interannual variability and predictability of two types of the El Niño–Southern Oscillation (ENSO), namely the canonical or eastern Pacific (EP)-type and Modoki or central Pacific (CP) type, are investigated. Using the retrospective forecasts of six-state-of-the-art coupled models and their multi-model ensemble (MME) for December–January–February during the period of 1972–2005 along with corresponding observed and reanalyzed data, we examine the climate regime shift that occurred in the winter of 1988/1989 and how the shift affected interannual variability and predictability of two types of ENSO for the two periods of 1972–1988 (hereafter PRE) and 1989–2005 (hereafter POST). The result first shows substantial interdecadal changes of observed sea surface temperature (SST) in mean state and variability over the western and central Pacific attributable to the significant

warming trend in the POST period. In the POST period, the SST variability increased (decreased) significantly over the western (eastern) Pacific. The MME realistically reproduces the observed interdecadal changes with 1- and 4-month forecast lead time. It is found that the CP-type ENSO was more prominent and predictable during the POST than the PRE period while there was no apparent difference in the variability and predictability of the EP-type ENSO between two periods. Note that the second empirical orthogonal function mode of the Pacific SST during the POST period represents the CP-type ENSO but that during the PRE period captures the ENSO transition phase. The MME better predicts the former than the latter. We also investigate distinctive regional impacts associated with the two types of ENSO during the two periods.

Keywords El Niño and Southern Oscillation (ENSO) · Climate regime shift · Decadal variability · Seasonal predictability and prediction · Multi-model ensemble (MME) · Teleconnection

H.-I. Jeong
APEC Climate Center (APCC), Pusan, Republic of Korea

H.-I. Jeong · J.-B. Ahn
Pusan National University, Pusan, Republic of Korea

J.-Y. Lee (✉)
Institute of Environmental Studies, Pusan National University,
Pusan 609-735, Republic of Korea
e-mail: juneyi@pusan.ac.kr

A. Alessandri
Agenzia Nazionale per le nuove Tecnologie, l'energia e lo
sviluppo economico sostenibile, Rome, Italy

A. Alessandri
University of Hawaii/International Pacific Research Center,
Honolulu, HI, USA

H. H. Hendon
Centre for Australian Weather and Climate Research, Bureau of
Meteorology, Melbourne, VIC, Australia

1 Introduction

Evidence has been emerging that a shift in the North Pacific basic climate occurred during the winter of 1988/1989 (Hare and Mantua 2000; Hollowed et al. 2001; Yasunaka and Hanawa 2003) in addition to the well-known climate shift in the tropical Pacific sea surface temperature (SST) together with other climate fields around the late 1970s (Nitta and Yamada 1989; Trenberth and Hurrell 1994; Graham 1992, 1994). Although the 1988/1989 climate regime shift was not as prominent as the one in the late 1970s, it was associated with significant changes in the atmosphere and ocean especially in the upper ocean including biology (Hare and

Mantua 2000). In particular, considerable changes were noted in the northern Pacific SST (Yeh et al. 2011b; Watanabe and Nitta 1999; Overland and Wang 2005; Maslanik et al. 1996; Walsh et al. 1996) during the winter of 1988/1989.

The late 1970s climate shift has received much attention, especially with regard to how the characteristics of ENSO changed (Gu and Philander 1997; Wang and Wang 1996; Wallace et al. 1998; Jia et al. 2012; Yu and Kao 2007). According to An and Wang (2000), the decade of 1962–1973 was characterized by high-frequency ENSO variability, while low-frequency variability was dominant for the decade of 1981–1992. Wu and Hsieh (2003) found greater nonlinearity of the ENSO cycle during 1981–1999 than during 1961–1975. An (2004) showed that the eastward propagation of SST anomaly (SSTA) at the onset of ENSO has been dominant since the late 1970s; while westward propagation was dominant before the 1970s. Tang et al. (2008) analyzed the prediction skill of three models, which showed a very consistent interdecadal variation, with high skill for the late twentieth century, and low skill for the period from 1900 to 1960. Furthermore, substantial changes in ENSO teleconnection patterns occurred after the regime shift in the late 1970s. Kodera (2010) revealed that the ENSO teleconnection pattern was characterized by a wave-train-like structure over the Pacific-American sector and propagates into the stratosphere for the pre-1978 period. However, for the post-1978, the ENSO teleconnection pattern was characterized by changes in the tropospheric subtropical jet.

Watanabe and Nitta (1999) investigated the decadal-scale climate changes in the mid- and high latitudes of the Northern Hemisphere in winter of 1988/1989 by using various observational data. They found a dipole pattern of height anomalies between midlatitude (warming) and Polar Region (cooling) was associated with reduction of the subtropical jet stream. As it is, the tropical Pacific decadal changes need not be associated with Pacific Decadal Oscillation (PDO) (Ashok et al. 2007), but various other potential factor exist (Yeh et al. 2009, 2011b). Yeh et al. (2011b) reexamined the 1988/1989 climate transition compared with 1976/1977 by highlighting characteristic changes in the SST variability. They found that the PDO-like SST variability played a dominant role in the 1976/1977 climate transition, while both the North Pacific Gyre Oscillation (NPGO)-like and PDO-like SST variability contributed to the 1988/1989 climate transition. From analysis of the Tropical Ocean and Global Atmosphere (TOGA) experiments, they suggested that the changes in the North Pacific atmosphere in the 1976/1977 climate transition were mostly driven by the tropics, whereas those in the 1988/1989 climate transition were not.

Recent studies have reported frequent occurrence of a different type of ENSO from the canonical one, namely ENSO Modoki or Central Pacific (CP)-type ENSO which has

the location of maximum SST anomalies shifted to central equatorial Pacific compared to the canonical or eastern Pacific (EP)-type one (Larkin and Harrison 2005; Ashok et al. 2007; Kug et al. 2009; Kao and Yu 2009; McPhaden et al. 2011). Climate impacts of the EP- and CP-type (or Modoki) ENSO are also distinctly different from each other especially over East Asia, Australia, and North America (Ashok et al. 2007; Weng et al. 2007; Wang and Hendon 2007; Ashok et al. 2009; Cai and Cowan 2009; Taschetto and England 2009; Lim et al. 2009; Weng et al. 2009; Jeong et al. 2012). Furthermore, there are evidences of increase in intensity as well as occurrence frequency of the CP-type ENSO since the 1990s (Lee and McPhaden 2010; Yeh et al. 2011a) attributable to either global warming (Yeh et al. 2009) or natural variability (Yeh et al. 2011a; Kim et al. 2012). Several studies also suggested that the frequency of the CP-type ENSO might increase in a warmer climate (e.g., Yeh et al. 2009; Kim and Yu 2012) in addition to changes in mean and variability of Tropical SST under anthropogenic global warming (e.g., Guilyardi et al. 2012; Stevenson et al. 2012; Lee and Wang 2014; Lee et al. 2014).

Understanding of the recent decadal change should be prerequisite to the study of future climate changes. Thus, the present study aims to understand how the interdecadal shift occurred in 1988/1989 modulated interannual variability and predictability of the two types of ENSO and their impact on regional climate. We focus on analyzing and predicting the two types of ENSO and their climate impact during boreal winter in the period of 1972–1988 (hereafter “PRE”) and 1989–2005 (hereafter “POST”). Specific questions to be addressed also include: (1) how well do current coupled models capture the observed interdecadal shift in mean climate and ENSO variability? and (2) How well do the current models forecast the interannual variability of the two types of ENSO and their different impact on regional climate in PRE and POST?

Section 2 gives a brief description of the multimodel forecast data and the multi-model ensemble (MME) methodology. In Sects. 3 and 4, we examine the ability of the MME to predict the decadal changes of two different types of ENSO events and report the prediction skill related to the regional impacts of the two types of ENSO changes in the Asia–Pacific. The last section comprises of a discussion and summary of this study.

2 Data and methodology

2.1 Hindcast and verification data

Retrospective seasonal forecasts (hindcasts) output from six coupled atmosphere–ocean climate models. The six coupled models are the POAMA2 model as contributed to

Table 1 Description of the coupled atmosphere–ocean climate models used

Institutes (model name)	AGCM (resolution)	OGCM (resolution)	Ensemble member	References
ECMWF (ECMF)	IFSCY31R1 (T159L62)	HOPE (0.3° × 1.4° L29)	9	Stockdale et al. (2011), Balmaseda et al. (2008)
UKMO (EGRR)	HadGEM2-A (N96L38)	HadGEM2-O (0.33°lat × 1°lon L20)	9	Collins et al. 2008
MF (LFPW)	ARPEGE4.6 (T63L31)	OPA8.2 (2°lat × 2°lon L31)	9	Daget et al. (2009), Salas-Méliea (2002)
IFM/GEOMAR (IFMK)	ECHAM5 (T63L31)	MPI-OMI (1.5°lat × 1.5°lon L40)	9	Keenlyside et al. (2005)
CMCC-INGV (INGV)	ECHAM5 (T63L19)	OPA8.2 (2°lat × 2°lon L31)	9	Alessandri et al. (2010)
BoM (P24A)	BAMv3.0d (T47L17)	ACOM2 (0.5°-1.5°lat × 2°lon L25)	11	Lim et al. (2012)

the Asia–Pacific Economic Cooperation Climate Center/Climate Prediction and its Application to Society (APCC/CliPAS) (Wang et al. 2009; Lee et al. 2010) and from the CMCC-INGV, ECMWF, IFM-GEOMAR, MF, and UKMO seasonal forecasts models as contributed to the ENSEMBLE-based predictions of climate changes and their impactS (ENSEMBLES) project (Weisheimer et al. 2009; Alessandri et al. 2011). None of the coupled models has flux adjustment. A brief description of the models and their references are provided in Table 1. We note that all models are initialized from observed atmosphere and ocean initial conditions and use ensemble forecasts to reduce uncertainties related to initial condition. For this study we use seasonal forecasts for the boreal winter (December–February) that are initialized on 1 November (e.g., 1 month lead) and 1 August (e.g., 4 months lead).

We form the MME using the simple composite method (Peng et al. 2002; Kang et al. 2009; Lee et al. 2008, 2011a, 2013). With this technique, equal weights are assigned to the ensemble mean predictions of each model, with the assumption that each model is independent. The mean bias from each model is removed by forming anomalies with respect to the each model’s own seasonal climatology. We focus on the period of 1972–2005.

The observed and reanalyzed datasets used for hindcast verification are the NOAA’s PRECipitation REConstruction dataset (PREC, Chen et al. 2002), the National Centers for Environmental Prediction (NCEP)-National Center for Atmospheric Research (NCAR) reanalysis 1 data (Kalnay et al. 1996) for atmospheric variables, and the Extended Reconstructed Sea Surface Temperature (ERSST.v3b) analyses (Smith et al. 2008).

2.2 Methodology

We compare the climatological mean differences of SST for 17 years in the two periods of PRE (1972–1988) and POST (1989–2005). We also examine the variance changes for SST and rainfall variability for the two periods. We

then carry out an Empirical Orthogonal Function (EOF) analysis to identify the observed dominant spatial patterns of SST anomalies in the tropical Pacific. The teleconnection patterns are then extracted using a linear regression analysis of observed rainfall on the principal components of the top two EOF modes, which represent the canonical and Modoki ENSO (e.g., Ashok et al. 2007). In order to examine the skill in predicting these observed features, we carry out similar analyses on the hindcasts of the MME. Pattern correlations are then employed to investigate the relationship between the observations and the coupled MME predictions for rainfall, in various regions surrounding the Pacific.

3 The observed and predicted decadal changes

3.1 Mean and variance

We investigate (1) whether mean and variance of SST and precipitation changed significantly in late 1980s and (2) how the coupled models and their MME capture the observed changes. Basically, the coupled models and their MME are able to reproduce the spatial distribution of observed mean SST although they still tend to have cold SST bias over the equatorial eastern Pacific and these are given in “Appendix”.

The differences of climatological winter (December through February, hereinafter DJF) mean between the POST and PRE for observed and predicted SSTs and their significance test for the climatological differences are presented in Fig. 1. There is a noticeable warming in the POST period, especially in the Indian, north Atlantic, and west Pacific Oceans, and the ocean in the vicinity of Korea and Japan (Fig. 1a). The MME successfully captures the warming over most regions in the Northern Hemisphere; however, there are significant warm biases over the Arctic Ocean in comparison with the observation. In addition, the 1-month MME fails to maintain the warm trend in the

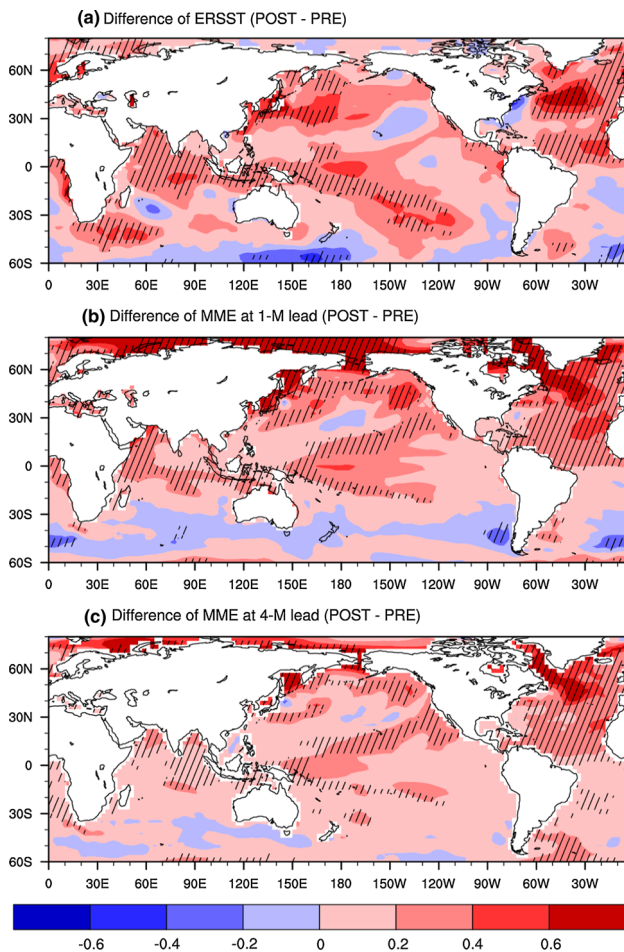


Fig. 1 a DJF climatological difference between 1989–2005 (POST) and 1972–1988 (PRE) of observed SST ($^{\circ}\text{C}$) and **b** one-month lead MME prediction. The slanted line areas indicate statistical significant difference at the 95 % confidence level from student's t test

tropical Indian Ocean. However, interestingly, we can find that this warming trend occurs at 4-month lead time.

Analysis of variance is a useful technique to understand the climate variability. To check changes in variability for the two periods, we present the variance of ensemble mean (signal), average of variances calculated from each ensemble member (total), and their ratio (signal to total) of observed and predicted SST and rainfall in Figs. 2 and 3, respectively. For the SST variability, there is maximum variability over the central to eastern Pacific and subtropical basin area (Fig. 2a) in observation. For the variance changes between two periods (Fig. 2b), the POST period shows significantly increased variability over the western Pacific including part of North Pacific and the North Atlantic Ocean and decreased variability in the south eastern Pacific.

The 1-month lead MME prediction well captures the area of maximum SST variability over the equatorial eastern Pacific (Fig. 2c), but variability is too weak off the

coast of South America, which is a common coupled model bias. Outside of the eastern Pacific, the MME tends to underestimate variance. There is lots of noise outside of the tropical Pacific, especially in North and South Pacific Ocean, southern part of Indian Ocean, and east coast of North America (Fig. 2e). In the ratios between the variances of the two periods (Fig. 2d, f), the MME successfully captures the area of major increase over the North Atlantic Ocean in the POST period. The MME also captures the increase/decrease in the equatorial west/central Pacific (Fig. 2d), but the pattern of changed variance is shifted to the west of the observed, again probably reflecting the typical bias in the representation of ENSO variability in coupled models (variability extends too far west; e.g., Hendon et al. 2009).

We estimate potential predictability in the forecasts of SST by the ratio of variance of the ensemble mean (signal) to average of variances calculated from each ensemble members (total variance) at Fig. 2g. The results indicate relatively high signal-to-total variance ratio in the tropical Pacific, which reflects the strong predictability arising from ENSO. Predictable signal is also found over the western Indian Ocean and tropical Atlantic Ocean, which probably reflect the strong teleconnections of the predictable ENSO signal in the Pacific to these basins (Shinoda et al. 2004; Shi et al. 2012). There is low potential predictability in the eastern tropical Indian Ocean indicating the Indian Ocean Dipole is less predictable than ENSO (e.g., Shi et al. 2012). Relatively low predictability is also seen in middle and high latitudes in both hemispheres. Interestingly, Fig. 2h shows that the signal is increased in POST compared to PRE over some parts of subtropics and middle latitudes and particularly in the far western Pacific in line with where the variability increases in the POST period (Fig. 2d).

The 4-month lead MME prediction successfully represents the maximum SST variability over the eastern tropical Pacific but there are some limitations in predicting the changes of variance between two periods over the North Atlantic Ocean and tropical Pacific. Over the western Pacific Ocean, the MME cannot reproduce the increasing variability but having decreasing variability for the more recent period (figures not shown).

Figure 3 represents the observed and predicted rainfall variance for the POST period and the variance ratio between the POST and PRE periods. In observation, the maximum variability of rainfall is shown over the warm pool area in SST mean field, where interannual variations are dominated by ENSO signals (Fig. 3a). We repeated the variance analysis with the Global Precipitation Climatology Project (GPCP) data (Adler et al. 2003) for the common POST period (1989–2005), and the results are well in agreement with that of NOAA PREC. The averaged variance calculated from each ensemble member (Fig. 3e)

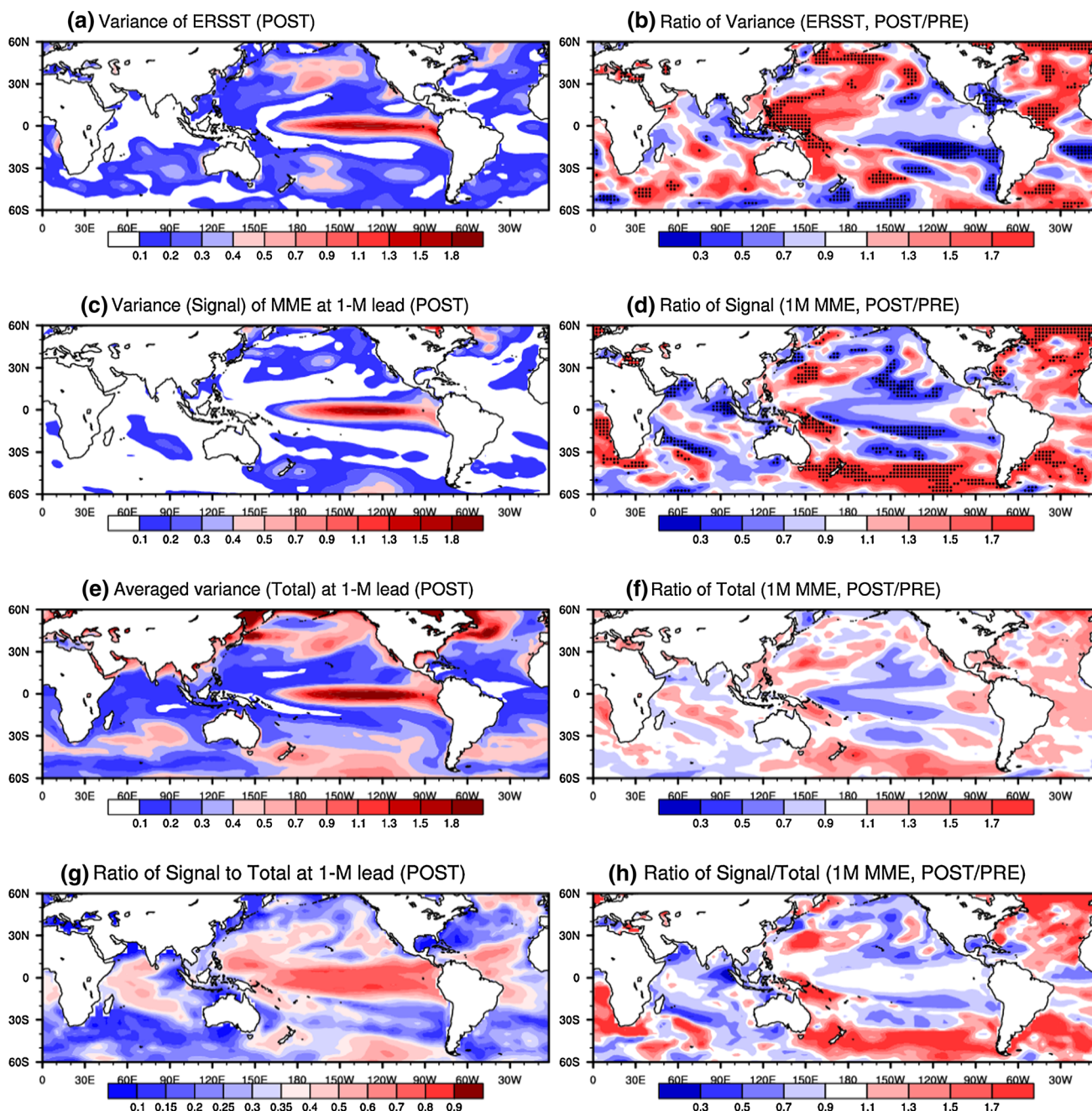


Fig. 2 Variance of SSTAs ($^{\circ}\text{C}^2$) in **a** observation and **c** MME predictions at 1-month lead, **e** average of each model member's variances, and **g** ratio of **c**–**e** for the period of POST (1989–2005). Right columns (from **b** to **h**) represent the ratio of POST (1989–2005)

to PRE (1972–1988) period in respect of left columns (from **a** to **g**). The stippled areas represent significant variance ratio at the 95 % confidence level from F test

overestimates variability over the western tropical Pacific and some part of Indian Ocean compared to observation. However, the MME prediction (Fig. 3c) at 1-month lead successfully simulates the variability of rainfall for the POST period over the western tropical Pacific. On the other hand, the MME prediction has limitations in predicting

rainfall variability precisely over land areas, and shows low variability over tropical South America (including Brazil), Northern Australia, and southeastern Africa (Fig. 3c) attributable to the models' deficiencies in parameterization of deep convection and representation of land process. Similar to the 1-month lead forecasts, the rainfall

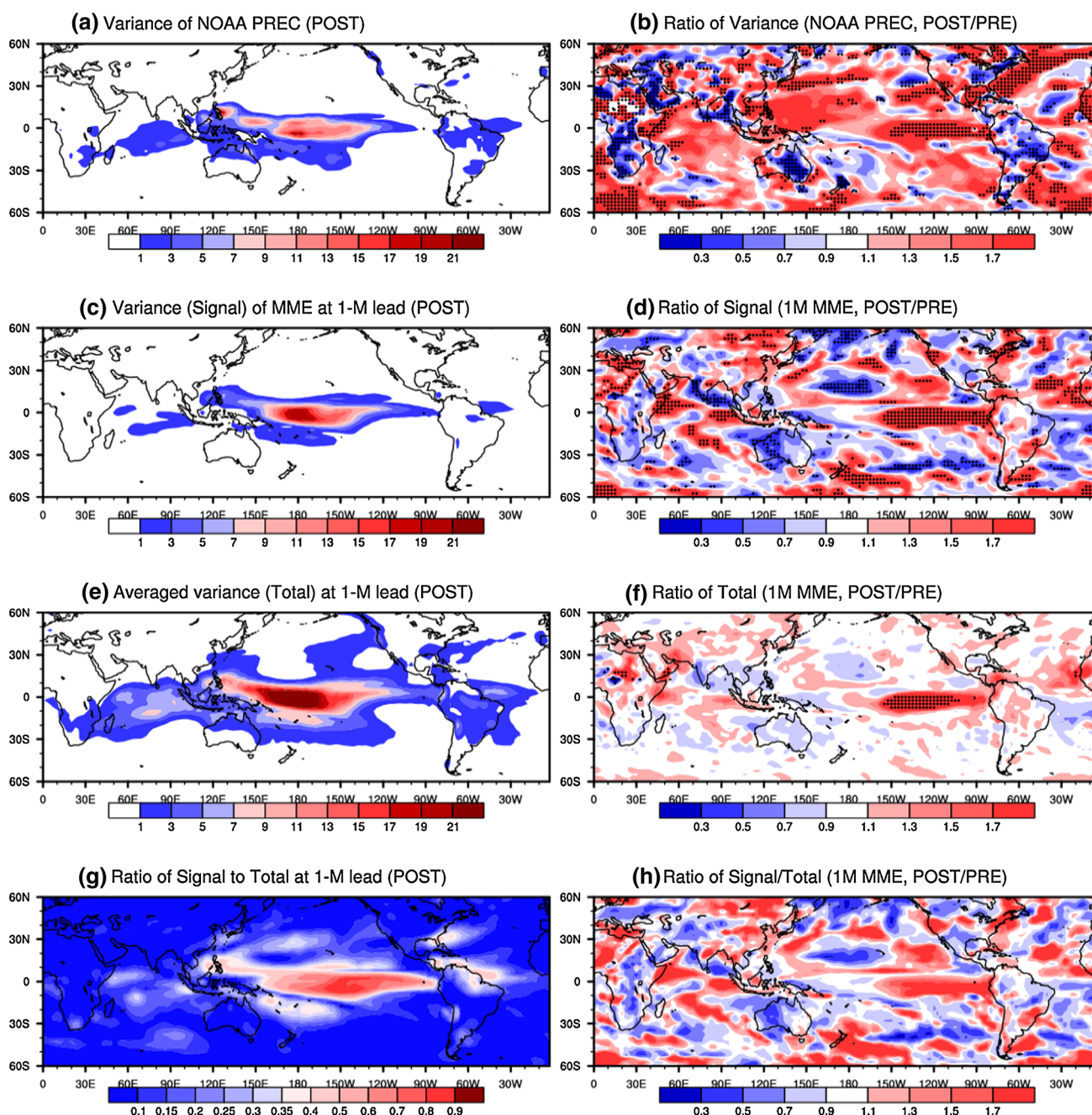


Fig. 3 Same as Fig. 2, except for rainfall (unit: mm^2/day^2)

variability of the 4-month-lead MME predictions is underestimated over land area, mainly due to cancellation of considerable noises over land area (figures not shown).

In the observed variance ratio of rainfall between POST and PRE periods (Fig. 3b), the POST period shows significantly larger variance in the North Pacific Ocean including equatorial eastern Pacific, most area of Indian Ocean including eastern part of Africa and Western Australia, and the eastern coast of North America. The rainfall variability is significantly reduced over eastern Australia in

the POST period which is consistent with a decline of ENSO variability in the equatorial Pacific (Fig. 2b). The MME prediction at 1-month lead successfully captures the positive change in the rainfall variance over the eastern tropical Pacific, some part of Indian Ocean and North Atlantic Ocean, while it simulates significantly decreased variability over Western Australia and some part of the North Pacific Ocean (Fig. 3d). Except for the eastern tropical Pacific, there are no significant changes in total variability for two periods (Fig. 3f). The 4-month lead

MME prediction captures the positive variance over the equatorial eastern Pacific, but the magnitude is much reduced as compared with that of 1-month lead MME prediction. Interestingly, the potential predictability as the ratio of signal to total variance at the 4-month lead is increased over equatorial eastern Pacific (figures not shown).

To sum up, the main features of 1988/1989 climate transition are the warming trend over most of the surface oceans, especially the western and central Pacific. The MME prediction successfully captures the warming trend over the most regions. It is also noted that SST variability is increased over the western Pacific but decreased over the eastern Pacific. However, the rainfall variability is much increased in the eastern tropical Pacific especially its eastern part. The coupled MME prediction also shows the similar level to observed changes over the tropics, although it tends to over or underestimate the observed features.

3.2 Prediction of the two major type of ENSO

We examine performance of the coupled MME in predicting the two types of ENSO at 1- and 4-month lead. In this study, the EP-type ENSO is represented by Niño3 SST index and CP-type ENSO by the EMI² index. Tables 2 and 3 show the anomaly correlation coefficients between observations and MME predictions for Niño3¹ and EMI² at 1- and 4-month lead, respectively, for the three different periods (total, PRE and POST periods). Considering the total period (1972–2005), the MME well predicts Niño3 and EMI at both 1- and 4-month lead time. The skill of EMI at 4-month lead even reaches above 0.7 and this correlation coefficient is exceeding significant value at 99 % confidence level from two-tailed Student's *t* test. The skill of Niño3 is robust despite of dividing into PRE and POST periods. On the other hand, the skill of EMI is better predicted during the POST than the PRE period especially at 4-month lead time.

3.3 The first EOF mode of tropical SSTA variability

We also assess predictability of two types of ENSO by analyzing leading EOF modes of SST variability in observation and MME prediction during the two periods. The leading modes of the observed DJF SSTA over the

Table 2 Anomaly correlation coefficient between observation and MME predictions for Niño3 index at 1- and 4-month lead time

ACC of Niño3	Total periods (1972–2005)	PRE (1972–1988)	POST (1989–2005)
1-M lead MME	0.97	0.97	0.98
4-M lead MME	0.92	0.91	0.93

Table 3 Same as Table 2, except for ENSO Modoki Index (EMI)

ACC of EMI	Total periods (1972–2005)	PRE (1972–1988)	POST (1989–2005)
1-M lead MME	0.85	0.81	0.91
4-M lead MME	0.75	0.69	0.82

tropical Pacific region (30°S–30°N, 120°E–60°W) for the two periods are presented in Fig. 4. The observed spatial patterns of the first EOF (EOF1) represent the well-known canonical EP-type ENSO pattern with the SSTA retaining the same sign throughout the equatorial eastern Pacific and with the maximum at about 155°W–115°W during both periods (Fig. 4a, b). The EOF1 explains 67.9 % (56.9 %) of the total variability for the PRE (POST) period. The percentage variance is reduced for the POST period by about 11 % in comparison with the PRE period, consistent with the overall drop in SST variability in the central and east Pacific during the POST period seen in Fig. 2b. However, the maximum SSTA over the equatorial eastern Pacific, at around 155°W–115°W, is strengthened during the POST period.

The ability of the MME to capture the EP-type ENSO mode is assessed by performing a similar EOF analysis on the MME hindcasts at 1- and 4-month lead times. The MME succeeds in capturing the spatial patterns of the first EOF modes at 1-month lead time, with high fidelity (Fig. 4c, d). The spatial correlations between the observed and predicted eigenvectors are 0.94 for the PRE and POST period. However, the variances explained by the EOF1 for the MME are 79.4 and 72.9 % (PRE and POST periods, respectively), indicating that the MME prediction explains a significantly larger amount of the variance than its observed counterpart. To check the amplitude of canonical ENSO for the two periods, we calculated the standard deviation of observed and predicted Niño3 at Table 4. Similar to the variances explained by the EOF1, the standard deviation of observed Niño3 during POST is little bit reduced compared to the PRE. Both MME predictions well match with that of observation. At 4-month lead time, the MME prediction also retains high fidelity in capturing the

¹ The Niño3 index is an area-average of the sea surface temperature in the region of 150°W–90°W and 5°S–5°N.

² The El Niño Modoki index or EMI is defined as $[SSTA]_C - 0.5[SSTA]_E - 0.5[SSTA]_W$, where the square bracket with a subscript represents the area-mean SSTA, averaged over one of the three regions specified as the central (C: 165°E–140°W, 10°S–10°N), eastern (E: 110°W–70°W, 15°S–5°N), and western (W: 125°E–145°E, 10°S–20°N).

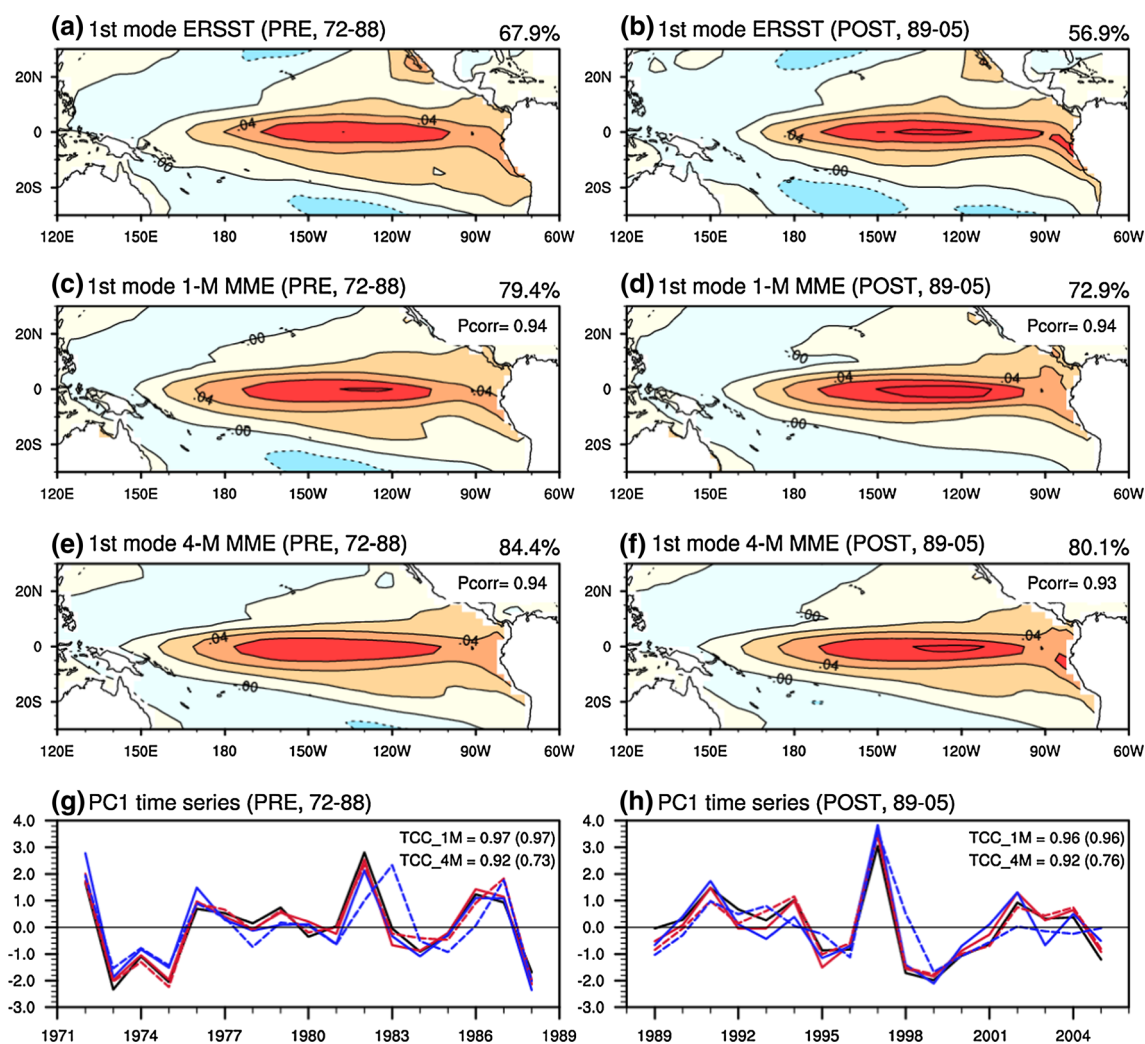


Fig. 4 Spatial patterns of the first EOF mode for **a, b** observed SSTAs over the tropical Pacific (30°S–30°N, 120°E–60°W) during the period of PRE (1972–1988) and POST (1989–2005). **c–f** are same as **a** and **b**, except for the MME predicted SSTAs at 1 and 4-month lead time. Pattern correlations between the observed and MME predicted spatial patterns of each EOF mode are given. **g, h** Principal component (PC) time series of the first EOF mode for observed (*black*

solid line) and MME predicted SSTAs at 1-month (*red solid line*) and 4-month (*blue solid line*) lead time during the period of PRE (1972–1988) and POST (1989–2005). *Dashed lines* are persistence skill of 1-month (*red*) and 4-month (*blue*) lead time. Time series are normalized by their respective standard deviation. Temporal correlations between observed and MME predicted PC1 time series are given and their persistence skills are presented in parenthesis

spatial pattern of the EOF1 (Fig. 4e, f). The spatial pattern correlation between the observed and predicted eigenvectors is 0.94 and 0.93 for the two periods, slightly less than the corresponding value at a 1-month lead for the POST period (Fig. 4f). The 4-month lead MME predictions have further increased the explained variance for the two periods.

The time series of the corresponding normalized PC1 for both the 1- and 4-month lead times during the two periods are presented in Fig. 4g, h. The PC1 from observations is well correlated at 0.97 (0.96) with that of the 1-month lead MME hindcasts for the PRE (POST) period. In general, at 1-month lead time, the persistence skill is slightly better than that of coupled prediction (Jin et al. 2008; Jeong et al.

Table 4 Standard deviation of Niño3 index for observation, 1- and 4-month lead MME predictions

STD of Niño3	PRE (1972–1988)	POST (1989–2005)
Observation	1.01	0.95
1-M lead MME	1.01	0.96
4-M lead MME	0.92	0.91

2012). However, we found that the persistence skills at 1-month lead time are the same as MME prediction for the PRE and POST periods showing 0.97 and 0.96, respectively.

Even at 4-month lead, the correlation of the PC1 is 0.92 for both periods. These are very highly correlated

compared to persistence skill of 0.73 (0.76) for the PRE (POST). The correlations at 4-month lead are also statistically significant at 99 % confidence level from the two-tailed Student's *t* test. It can be discerned that the MME successfully predicts both the spatial structure and the temporal behavior of the first EOF of SST at 1- and 4-month lead during PRE and POST periods.

3.4 The second EOF mode of tropical SSTA variability

It is interesting to note that there are distinct changes in the second EOF (EOF2) of observed SSTA between the two periods shown in Fig. 5a, b. The EOF2 in the POST period (Fig. 5b) shows the maximum variability near the dateline, and is flanked by opposite signed anomalies in the far eastern and far western Pacific similar to the Modoki or CP-type ENSO (Ashok et al. 2007; Hendon et al. 2009). The EOF2 pattern shows that there is strong connection

with the Northeast Pacific (Fig. 5b). Actually, there are some evidences for connection between CP-type ENSO (or Modoki) and North Pacific behaviors. Yu et al. (2012a) also identified that there is relationship between tropical central Pacific SST variability and the extratropical atmosphere around 1990. They concluded that the North Pacific Oscillation (NPO) mode of extratropical SLP variations has exerted a strong influence on SST variations in the tropical central Pacific since 1990.

On the other hand, in the PRE period, the EOF2 does not show any clear maximum variance in the central tropical Pacific, and bears a visible resemblance to the features of ENSO transition. Though the ENSO transition usually occurs at spring and summer season, we found two cases of 83/84 and 85/86 winter season (DJF) as ENSO transition time during the PRE period.

Ashok et al. (2007) compared the tropical SSTA variability before and after 1979 and claim that the ENSO

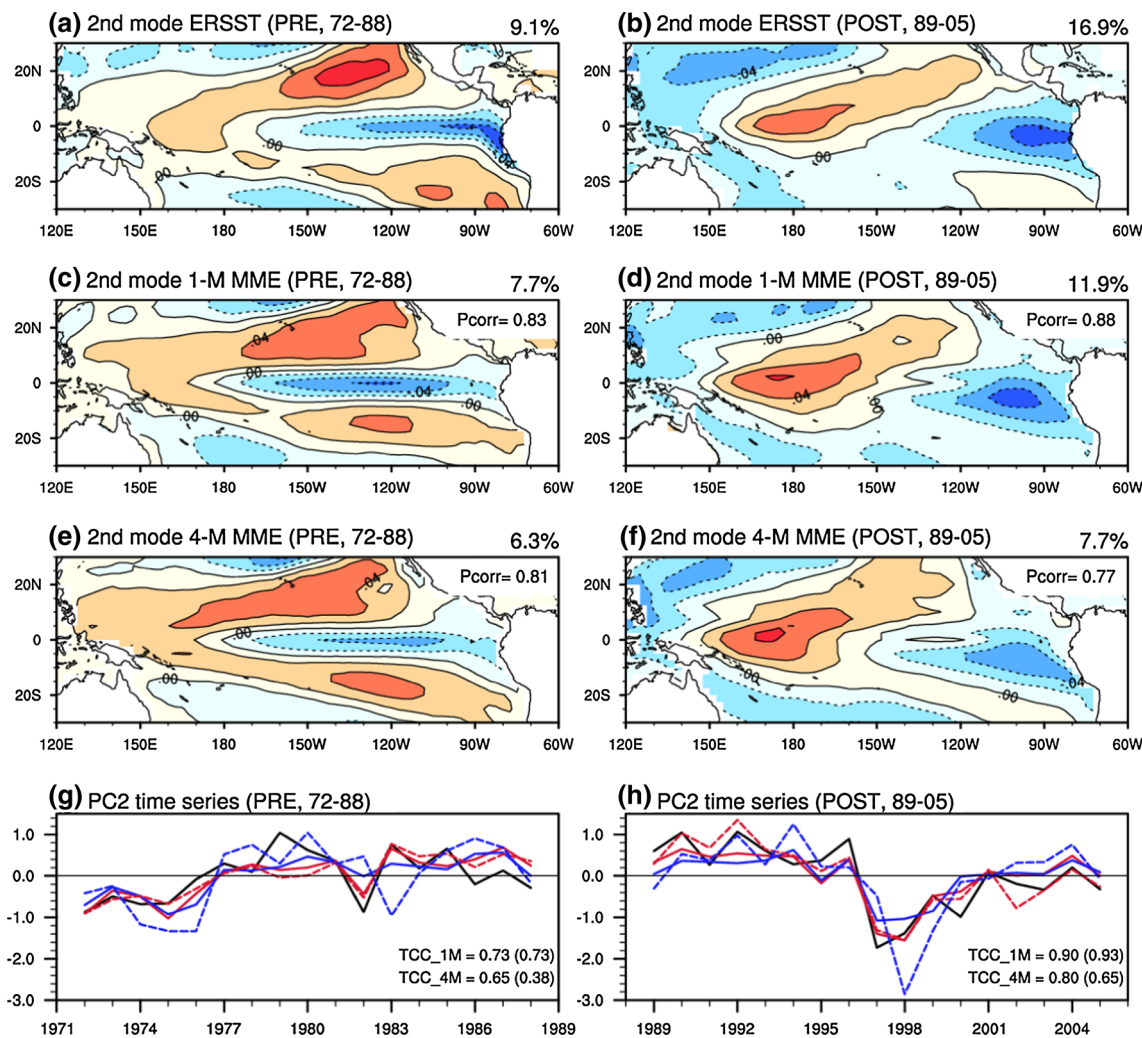


Fig. 5 Same as Fig. 4, except for the second EOF mode

Table 5 Same as Table 4, except for ENSO Modoki Index (EMI)

STD of EMI	PRE (1972–1988)	POST (1989–2005)
Observation	0.39	0.58
1-M lead MME	0.48	0.46
4-M lead MME	0.39	0.36

Modoki mode is not represented in the second EOF mode before 1979. Further, they claim that the ENSO Modoki mode only appears after 1979. Their conclusion is consistent with the increase of explained variance by EOF2 from 9.1 % in PRE to 16.9 % in POST period. It is also found that the standard deviation of observed EMI has been much increased at the POST compared to the PRE (see Table 5).

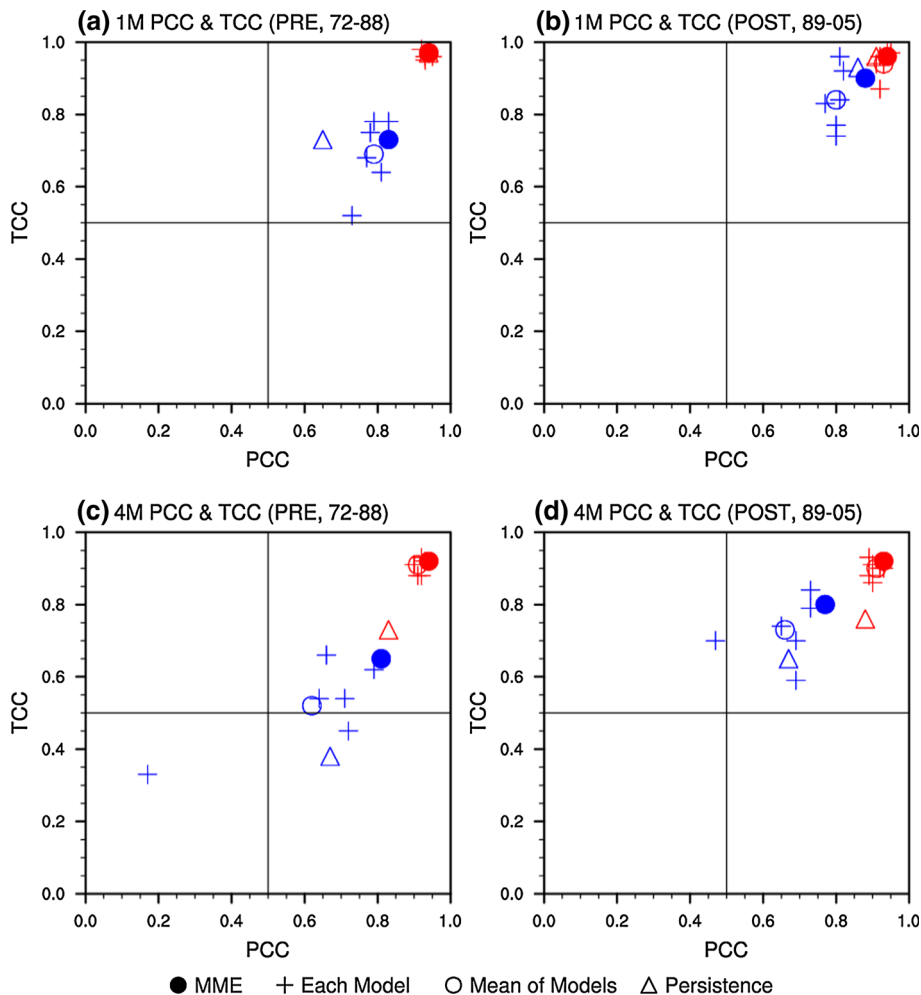
The MME at 1-month lead successfully captures the second EOF mode, showing a high spatial pattern correlation of 0.83(0.88) for the PRE (POST) period. The variance explained by the MME hindcasts also increases during the POST period compared to PRE. However, the MME tends to underestimate the amplitude of ENSO

Modoki with respect to observations. This is also found that MME prediction underestimates the standard deviation of EMI compared to the observation for the POST (see Table 5).

At 4-month lead, the spatial pattern correlations between the observed and predicted eigenvectors are 0.81 and 0.77 for PRE and POST, respectively, thus, slightly decreasing compared with the corresponding values in the 1-month lead. The spatial pattern of the EOF2 for the POST period indicates a strengthened central tropical Pacific and a weakened eastern equatorial Pacific variability, compared with that of the observation. The variance explained by the EOF2 from the 4-month lead MME forecasts has further reduced to 6.3 and 7.7 % for the PRE and POST periods, respectively.

It is noted that the MME for the EOF2 during the POST period has better skill than that during PRE. PC2 from observations is correlated at 0.73 (0.65) with PC2 from the MME at 1- (4-month) lead time for the PRE period. For the POST period, the temporal correlation of PC2 increases to 0.90 (0.80) at 1- and 4-month lead time. Interestingly, the

Fig. 6 Scatter diagram between the spatial pattern correlation coefficients (PCC) of eigenvectors and temporal correlation coefficients (TCC) of principal components for the first (red) and second (blue) EOF modes of SSTAs over the tropical Pacific (30°S–30°N, 120°E–60°W) during the period of PRE (1972–1988) and POST (1989–2005). The top and bottom panels are at 1 and 4-month lead time



persistence skills are also much improved during the POST period at both lead times. Even at 4-month lead time, the correlations are statistically significant at 99 % confidence level from two-tailed Student's *t* test.

3.5 Performance of individual models for tropical SSTA variability

We examine performance of individual models in predicting the dominant spatial patterns and temporal behavior of the first two leading EOF modes of the SSTAs at 1- and 4-month lead time for the two periods, and compare the results with those of the MME predictions (Fig. 6). The prediction skills of some individual models are slightly higher than that of the MME (especially, temporal correlations of PC2 in Fig. 6a, b). However, it can be seen that the overall skill of the MME is superior to those of individual models in the spatial (temporal) correlation of the EOF2 pattern (PC2 time series) of SSTAs at 1- and 4-month lead. Also, the MME's skill is better than the

averaged skill of individual models and the persistence skills. It is interesting to note that the individual models and their MME skill for the EOF2 at both 1- and 4-month lead have higher skill in capturing both spatial and temporal variation during the POST period than the PRE period, while they have similar skill for the EOF1 during the two periods.

Some improvement of the forecasts skill for the recent climate might be because of an increasingly improved observing system from past to recent years for both the ocean and atmosphere from which initial conditions for the forecasts are derived. According to Behringer and Xue (2004), the ocean observing instruments have increased dramatically since the early 1990s. Recently, Jia et al. (2014) examined the impact of the initial condition of coupled GCM on the interdecadal change of seasonal predictability. They have shown some increase of the seasonal forecast skill at the recent period compared to the older one. However, it appears that the key cause of the change in predictability is due to the commensurate change in variability.

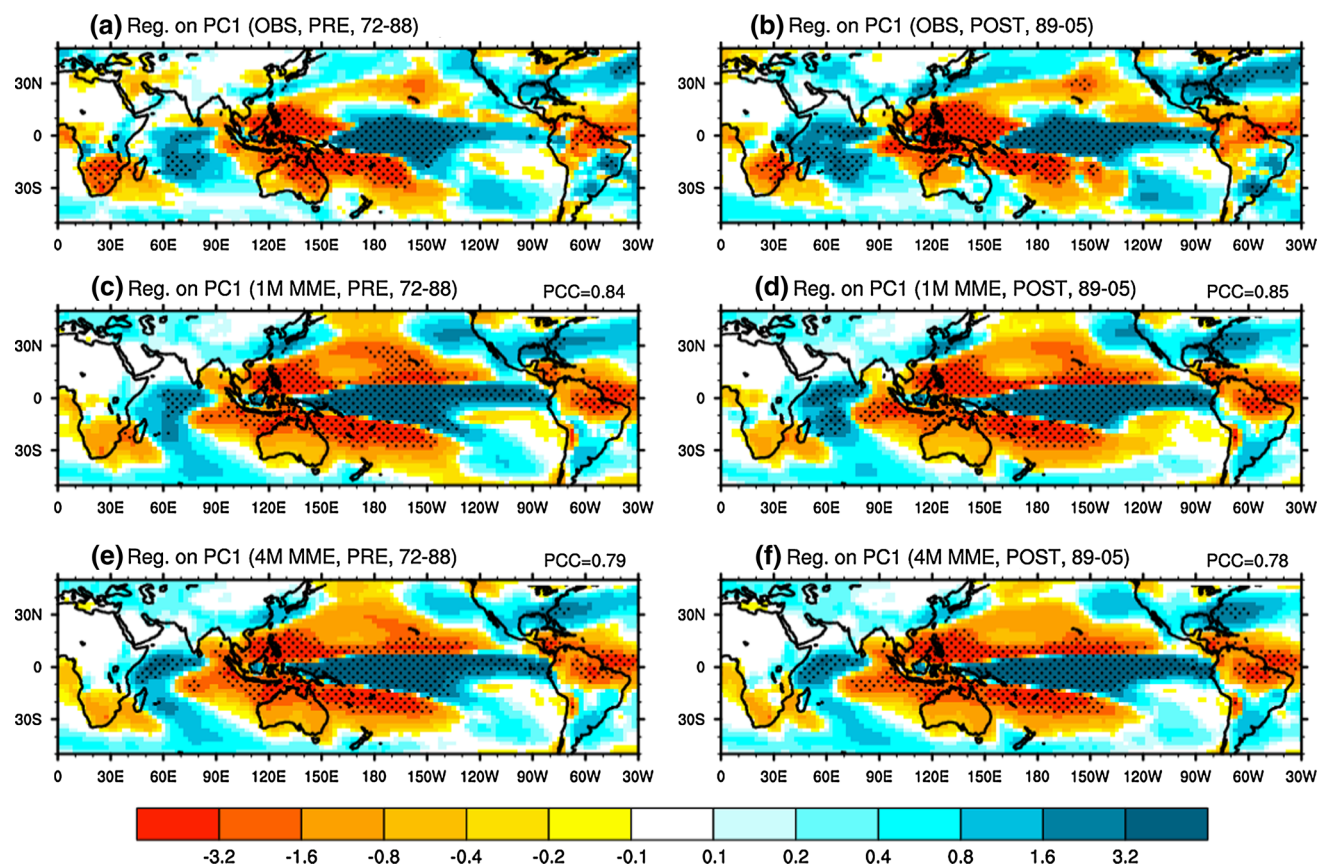


Fig. 7 Regression patterns of **a, b** observed rainfall anomalies (unit: mm day⁻¹) based on PC time series (see Fig. 4) of the first EOF mode for observed SSTA during the period of PRE (1972–1988) and POST (1989–2005). **c–f** are same as **a** and **b**, except for the MME prediction

at a 1 and 4-month lead time, respectively. The stippled areas represent significant regression coefficients at the 95 % confidence level from student's *t* test

4 Regional impact by the changes in the major modes

As shown in the previous section, the MME prediction at 1- and 4-month lead is able to capture the first two leading modes of tropical Pacific SSTA variability. In this section, we briefly revisit the distinctive impacts of the two types of ENSO around the Pacific Rim, and examine how the coupled MME performs in predicting the observed impacts during the two periods.

4.1 First mode of EOF

To find the linear relationships between rainfall (500 hPa geopotential height) and tropical SST variability, we examine regression map of rainfall (500 hPa geopotential height) anomalies onto the standardized PC1 (Fig. 4g, h) calculated from EOF analysis in Figs. 7 and 8.

In association with the EP-type ENSO (Fig. 7a, b), positive rainfall anomalies are observed over the

Intertropical Convergence Zone (ITCZ) in the eastern and central Pacific, flanked to the west by a broad horse-shoe shaped negative rainfall anomaly centered in the western tropical Pacific that extends eastward into the northern and southern Pacific. Anomalous dry conditions are seen in the South Pacific Convergence Zone (SPCZ), Maritime continent, western tropical Pacific and the Philippines (in agreement with Weng et al. 2009). Dry conditions also exist over tropical South America. Such below normal rainfall conditions are shown in both the PRE and POST periods, and this feature is well documented in earlier studies (Ropelewski and Halpert 1987, 1989; Diaz et al. 2001; Saji and Yamagata 2003; Ashok et al. 2007). An anomalous dry condition is seen over most of Australia in the PRE period, and is more significant in eastern and northern Australia. However, during the POST period, the anomalous dry condition over Australia is weakened and contracts to the west, while wet (but not significant) anomalies occur over eastern Australia. During the POST

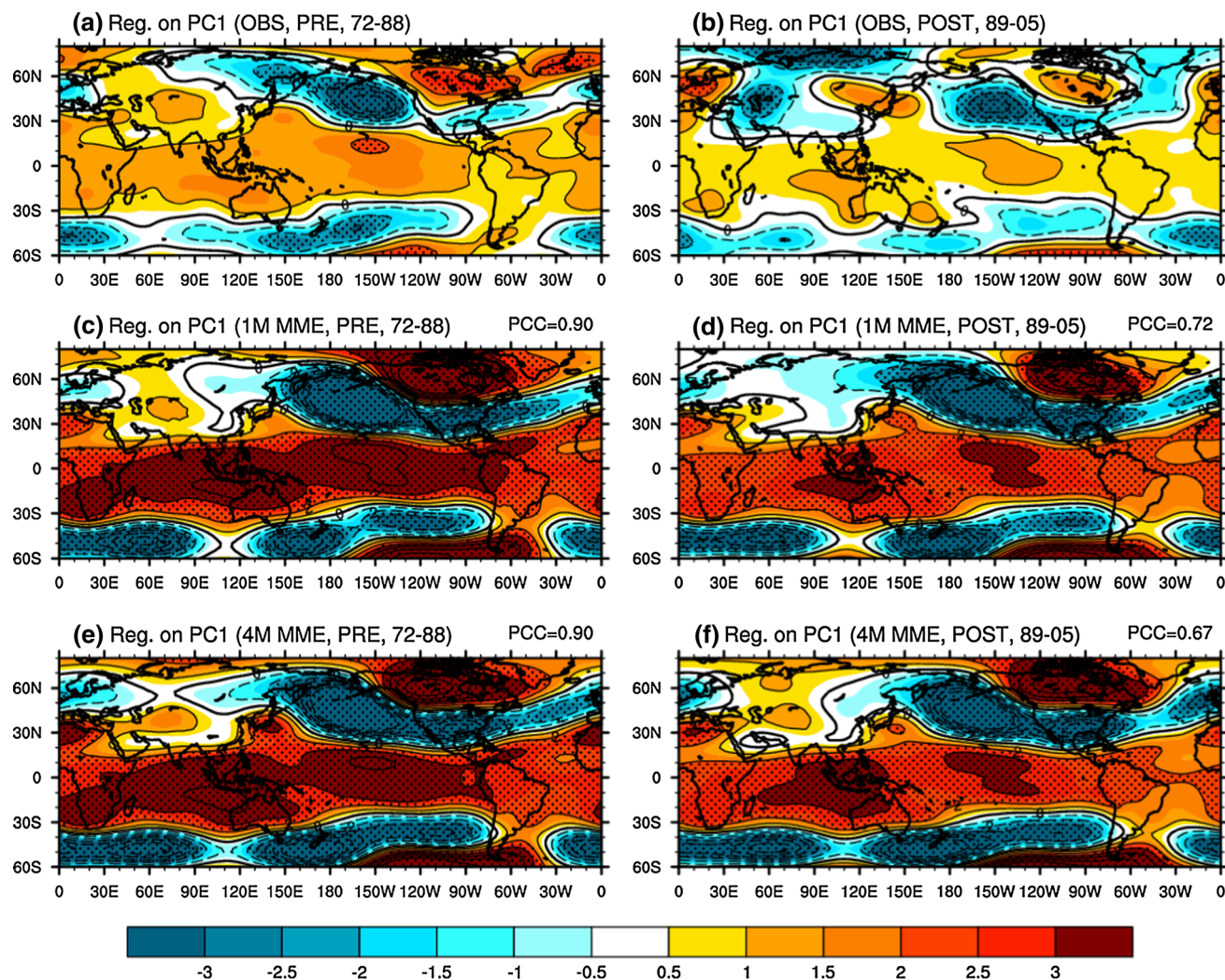


Fig. 8 Same as Fig. 7 except for normalized 500-hPa geopotential height anomalies. Contour interval is 1

period, there is also an anomalously strong and intensified winter monsoon rain band over the southern part of North America, into the North Atlantic Ocean and over most of the Indian Ocean (Fig. 7b).

We assess now how well the MME can predict these rainfall features associated with SST EOF1. The regression pattern of the hindcast rainfall onto PC1 at 1- and 4-month lead time for the two periods is shown in Fig. 7c–f, respectively. In general, the MME prediction replicates the observed features well. For example, the anomalously strong monsoon rainfall in East Asia and the anomalously wet (dry) conditions over North (tropical South) America are well represented for the two periods (PCC is 0.84 (0.85) for the PRE (POST) period). However, wet conditions in the equatorial Pacific extend further to the west into the Maritime continents, which we attribute to a systematic model bias in the representation of the canonical El Niño (e.g., Jeong et al. 2012). At 4-month lead time, the regression patterns of rainfall are very similar to those of 1-month lead time. The dipole mode that shows wet and dry conditions over the Indian Ocean is a predominant feature, and the whole of Australia shows anomalously dry conditions but the significant signal does not extend far

enough south during the PRE period (PCC is 0.79 (0.78) for the PRE (POST) period). The MME predictions at 1- and 4-month lead successfully capture the intensified rainfall anomalies over the southern part of North America for the POST period.

To investigate the decadal change of teleconnection pattern at the middle latitudes, we present the standardized regression coefficients of 500 hPa geopotential height anomalies onto PC1 (Fig. 8). The observed pattern of anomalous 500 hPa geopotential height shows the poleward wave train pattern (in agreement with Yu et al. 2012b) from equatorial Pacific to northern part of North America for both periods (Fig. 8a, b). However, for the POST period, the regression coefficients over tropics are much reduced compared to the PRE period. The MME predictions are well matched with poleward wave train pattern from equatorial Pacific to North America at 1- and 4-month lead time during the PRE and POST period. However, there are some limitations in predicting significantly the anomalous geopotential height pattern over the Eurasian continent. Surprisingly, the MME predictions well represent the weakened regression pattern over tropics for the POST period similarly to the observation.

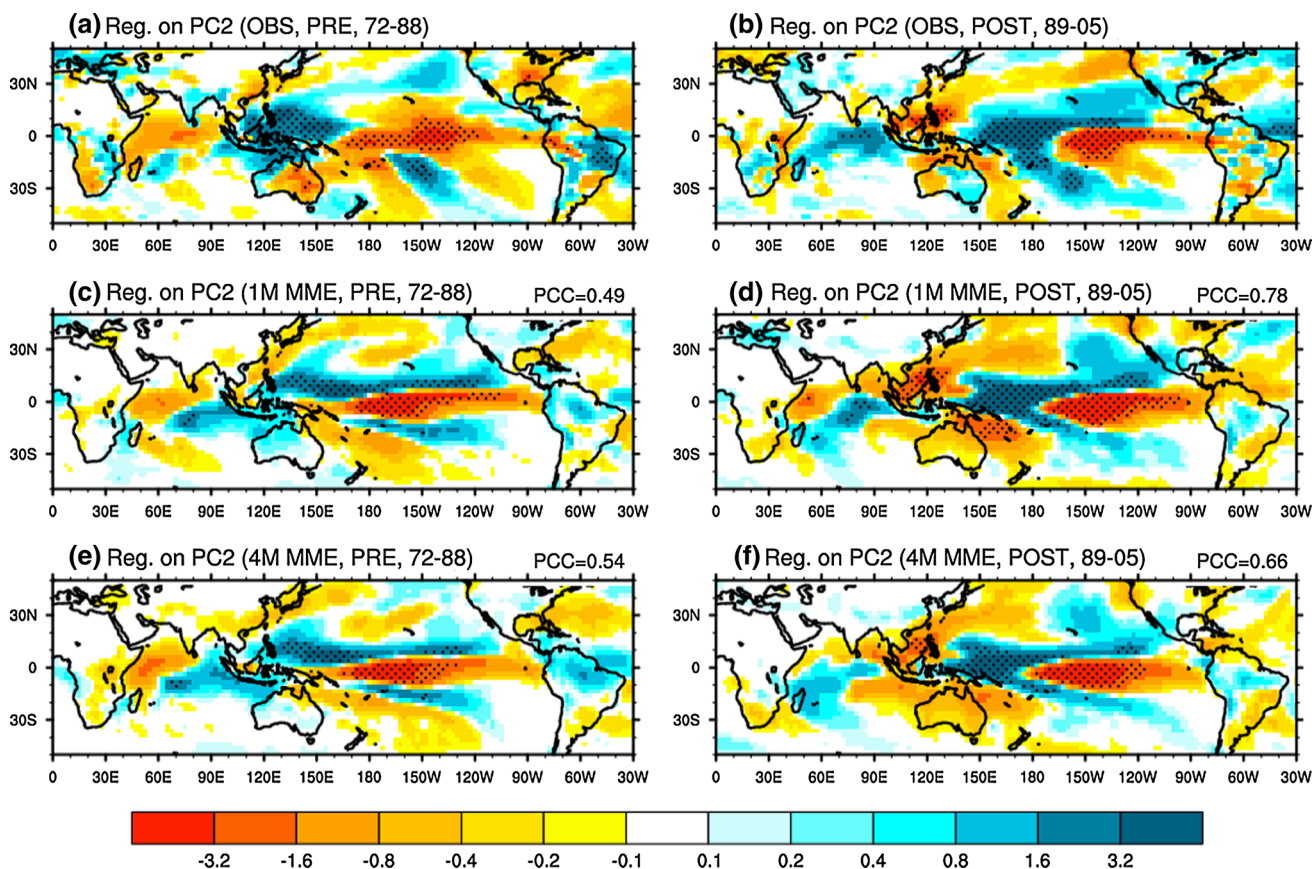


Fig. 9 Same as Fig. 7, except for PC time series of the second EOF mode

4.2 Second mode of EOF

To investigate the linear relationships between rainfall (500 hPa geopotential height) and tropical SST variability, we also examine regression map of rainfall (500 hPa geopotential height) anomalies on to the standardized PC2 calculated from EOF analysis (Fig. 5g, h) in Figs. 9 and 10. It is noted that there are significant changes in the regional impact of the EOF2 from PRE to POST.

During the PRE period, positive rainfall anomalies over the western tropical Pacific including the Maritime continents, Western Australia and the Philippines are observed. Similarly, other positive rainfall anomalies are over the ocean adjoining Polynesia at around 150°W, 20°S. Dry conditions exist over the Indian Ocean, but these are not significant. In contrast, the POST period reveals anomalously wet (dry) conditions to the west of the dateline

(equatorial eastern Pacific). It is noteworthy that the signs between the PRE and POST period are completely different over the Indian Ocean, western Pacific including Maritime continents, and Australian continent. During the POST period (ENSO Modoki), the winter monsoon in central eastern China is anomalously weak, whereas it is quite strong during canonical El Niño (Fig. 7b). The anomalous rainfall associated with the two tropical Pacific phenomena during the POST period is also opposite to one another in East Asia. These findings are in agreement with Weng et al. (2009).

The observed tripole mode associated with the second EOF mode over the equatorial Pacific is well predicted respectively by the 1- and 4-month lead predictions in the POST period showing the pattern correlation coefficients of 0.78 and 0.66 (Fig. 9b, d, f). Moreover, the MME predictions at both lead times successfully predict the

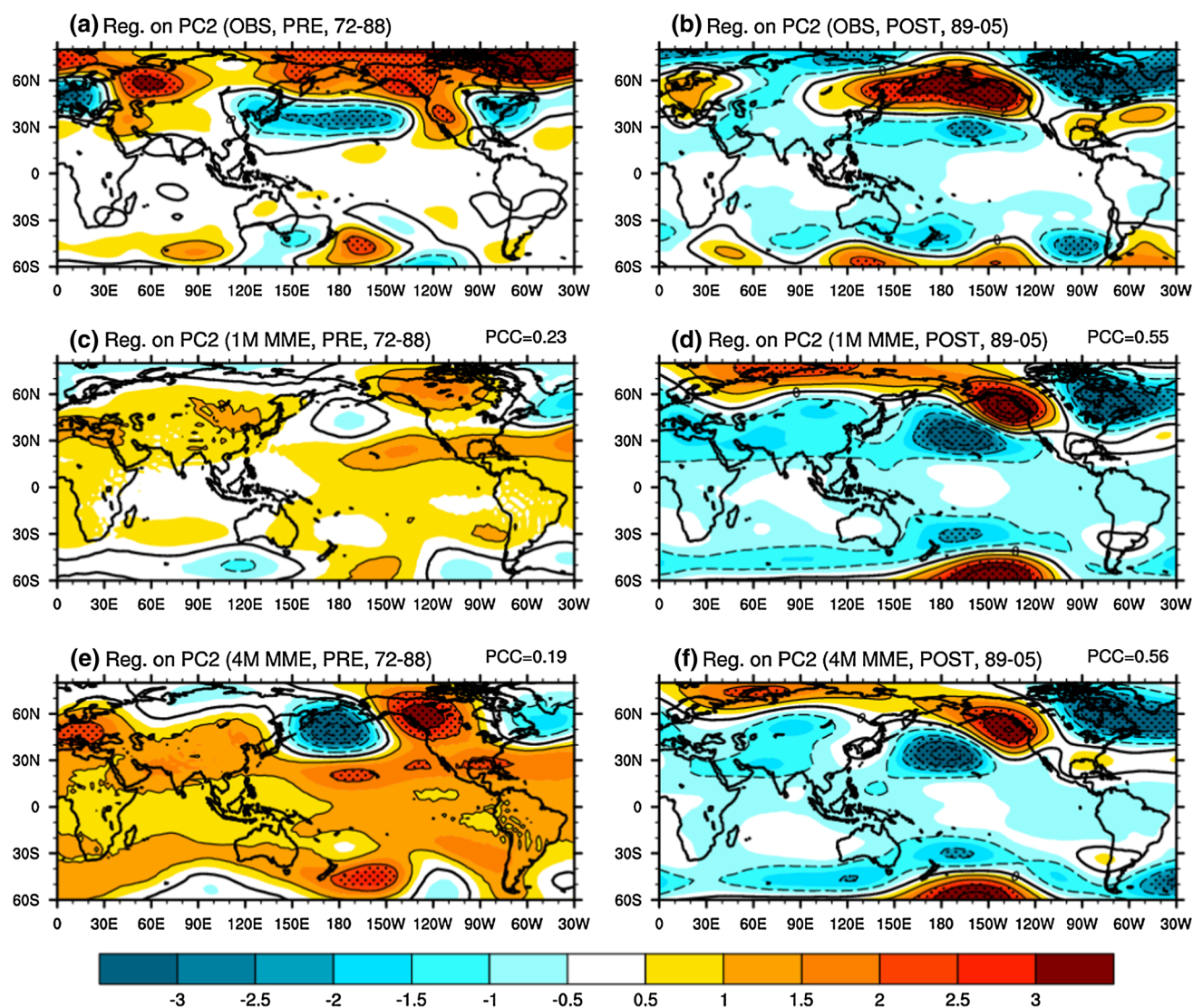
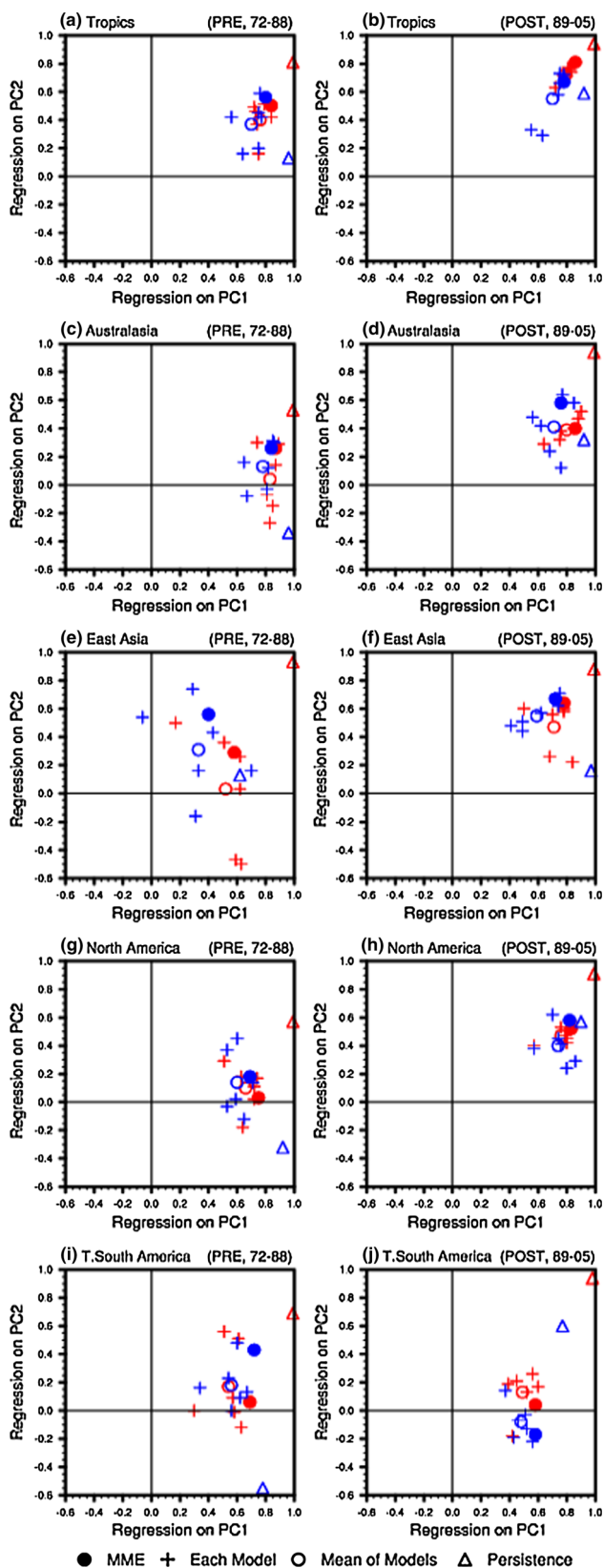


Fig. 10 Same as Fig. 8, except for PC time series of the second EOF mode



◀**Fig. 11** Scatter diagram of the pattern correlation coefficients between regressed patterns of observed and simulated EOF modes for observed and predicted SSTAs at 1-month (*red*) and 4-month (*blue*) lead time over the five regions of the Tropics (30°S–30°N, 0–360°E), Australasia (45°S–10°S, 110°E–180°E), East Asia (20°N–60°N, 90°E–150°E), North America (20°N–60°N, 140°W–50°W), and tropical South America (15°S–10°N, 80°W–35°W). The left panels represent for the PRE (1972–1988) period and the right panels represent for the POST (1989–2005) period

anomalously weakened winter monsoon from Sumatra to southern Japan. However, the observed anomalously wet conditions over SPCZ are not correctly simulated. During the PRE period, the observed dipole over the equatorial western and central Pacific is not well represented in 1- and 4-month lead MME predictions. There are further limitations in predicting the rainfall anomalies over the Indian Ocean, showing the dipole mode at both lead times (PCC is 0.49 (0.54) at 1- (4-month) lead time).

In terms of teleconnection pattern of 500 hPa geopotential height anomalies related with the second EOF mode of SST variability in the middle latitudes, there are significant decadal changes over the northern hemisphere. During the PRE period, there are some significantly negative anomalies around the North Pacific (180°, 40°N). They propagate to the North America consisting of a positive anomaly center extended from Alaska to western US and a negative anomaly center over eastern US (Fig. 10a).

On the other hand, in the POST period, the regression pattern of geopotential height anomalies is totally different from the PRE period showing the Pacific North America pattern (Wallace and Gutzler 1981; Yu et al. 2012b). US and southern part of Canada experiences warm-cold (warm) conditions during the PRE (POST) period. Besides on this, during the POST period, Eurasia continents and northern part of North America experiences opposite climate compared to PRE period. Unfortunately, the MME forecasts fail to predict the teleconnection pattern for the PRE period at 1- and 4-month lead time showing the pattern correlation of 0.23 and 0.19, respectively. Even at 1-month lead time, there are few signals in MME prediction. However, at the POST period, the MME prediction has some skill in predicting the main features of PNA pattern over the Pacific and North America at both lead times.

4.3 Forecast skills for regional impacts: MME versus individual models

Previous studies have demonstrated that the ENSO is the major predictability source for regional climate forecasts

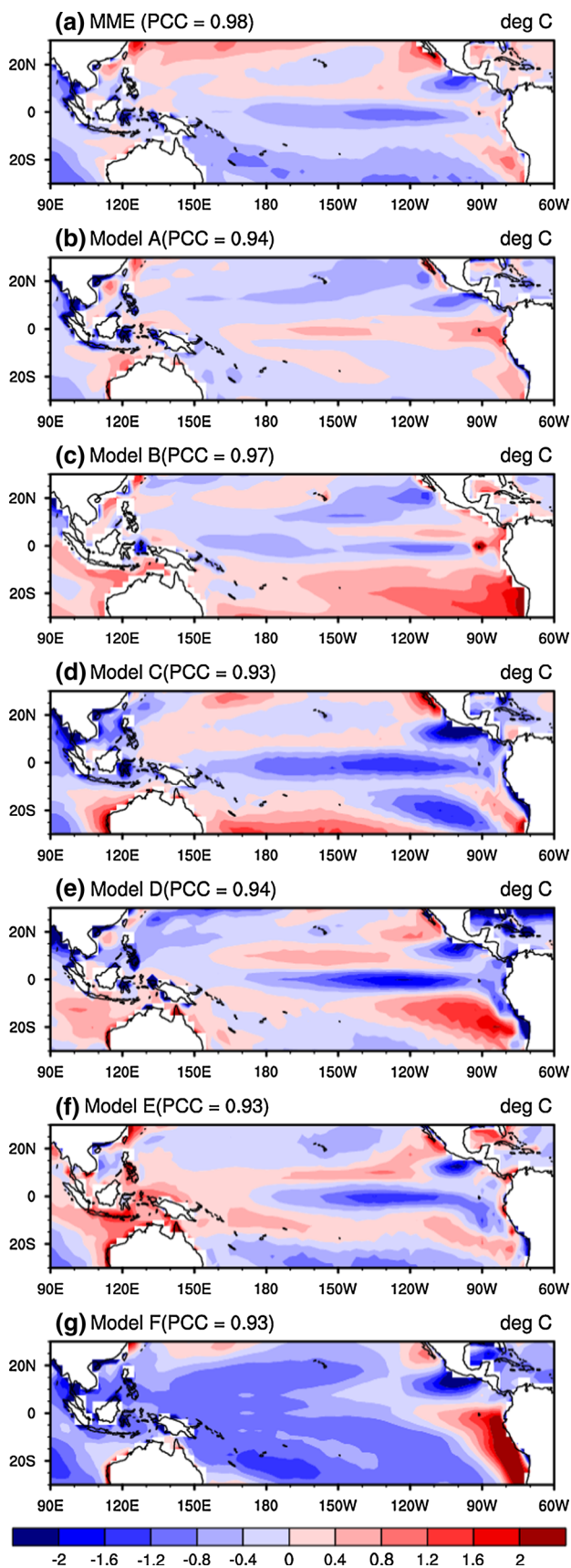


Fig. 12 DJF difference between observed mean SST and one-month lead MME prediction (a) and individual models (b–g) for 1972–2005. Pattern correlation coefficients between the observed and model predicted mean SST are also given at the top of each figure

(Wang et al. 2008a, b, 2009; Lee et al. 2010, 2011b, c, and many others). Thus, it is important that coupled models are able to capture the regional impacts of ENSO. In order to quantify the skills of the MME in predicting the impacts of the two types of ENSO at 1- and 4-month lead time, we present the prediction skills of the MME and six individual models for the regional impact, especially for regressed rainfall, in Fig. 11. These are based on the first two leading EOF modes of the observed and predicted SSTA at 1- and 4-month lead time over the five different regions, namely the Tropics (30°S – 30°N , 0 – 360°E), Australasia (45°S – 10°S , 110°E – 180°E), East Asia (20°N – 60°N , 90°E – 150°E), North America (20°N – 60°N , 140°W – 50°W), and tropical South America (15°S – 10°N , 80°W – 35°W). The mean of the prediction skills of the individual models and the persistence skills are also calculated. As indicated in Fig. 11, at 1-month lead time the predictive skill of the MME is significantly better in predicting the EP-type ENSO-associated impacts, compared with the impacts of the CP-type ENSO, (except for East Asia). Specifically, the pattern correlation coefficient for rainfall associated with the canonical ENSO reaches approximately 0.6 for these four regions during the two periods. In contrast, in East Asia, a CP-type ENSO-associated impact is better predicted at a 4-month lead. In general, the 4-month lead MME prediction for rainfall anomaly exhibits a poorer performance than the 1-month lead MME predictions. However, in this study, the skills for the 4-month lead MME predictions are comparable to those of the 1-month MME predictions for the five above-mentioned regions. As shown in Fig. 11, better prediction skills are evident in the POST period than in the PRE period. Interestingly, the persistence skills associated with the canonical ENSO are nearly perfect for the PRE and POST periods at both lead times. For the skills associated with the CP-type ENSO, in general, MME prediction beats the persistent forecast.

5 Summary and conclusions

The main purpose of this study is to understand the impacts of the decadal shift that occurred during 1988/1989 on tropical SST variability and predictability associated with ENSO. To investigate the predictability of tropical SST, we used reforecast data from the ENSEMBLES and POAMA forecast systems for the boreal winter season (DJF) during the period of 1972–2005.

Our main conclusions are as follows:

- The main feature of 1988/1989 climate transition is the warming trend over the western and central Pacific Ocean. Commensurate with this shift, SST variance increased over the western Pacific and decreased over the eastern Pacific Ocean. However, rainfall variability intensified in the central Pacific for the recent epoch. The coupled MME predictions well reproduce these observed changes.
- Examining the performance of two types of ENSO for the two periods, it is found that the coupled MME well predicts the Niño3 and ENSO Modoki index (EMI), which are representative indices for the canonical El Niño and ENSO Modoki, respectively. During the POST period improved predictability of the EMI is consistent with an increase of SST variance in the western Pacific.
- The spatial and temporal behavior of the second EOF of SST during the POST period is more predictable than those during the PRE period. In addition, the teleconnection related with the PC2 is also better captured, which are consistent with the emergence of ENSO Modoki during the POST period. In other words, these results show that the capability of the MME prediction for the tele connection related to ENSO Modoki may contribute to the enhancement of forecasts performance in the POST period.

Even though we did not discuss in this study, we also considered and analyzed another climate regime shift such as before and after the late 1970s. There is no special change on rainfall anomalies associated with the first mode of SST variability between the late 1970s and the late 1980s as two climate regime shifts. However, as compared with the second mode of SST variability, the intensity of the rainfall anomaly pattern shows more apparently for climate before the late 1980s (PRE period in this study) than before the late 1970s over Maritime continents including Philippine and equatorial central Pacific.

Our analysis focused on the tropical Pacific SST variability and their teleconnections. Actually, according to Yeh et al. (2011b), the climate regime shift during the late 1980s occurred over North Pacific rather than over the tropical Pacific. The decadal variability and predictability related with changes in the SST variability of the North Pacific need to be analyzed in the future study.

Acknowledgments We appreciate the anonymous three reviewers for their helpful comments and suggestions. This research was carried out in APEC Climate Center which is fully funded by Korea Meteorological Administration (KMA), Republic of Korea. J.-B. Ahn was supported by Rural Development Administration Cooperative Research Program for Agriculture Science and Technology Development under Grant Project No. PJ009953, Republic of Korea. A. Alessandri was partially supported by the European Commission's Seventh Framework Research Programme projects CLIMITS under

the grant agreement 303208 and SPECS under the grant agreement 308378. This work was also supported by IPRC, which is supported in part by JAMSTEC, NOAA, and NASA. This is the SOEST publication number 9070 and IPRC publication number 1042.

Appendix

The DJF differences between observed and predicted mean SST are shown in Fig. 12. Most of individual models and MME prediction have a cold bias over the equatorial eastern Pacific. On the other hands, the coupled models and their MME well reproduce the spatial distribution of observed mean SST showing higher skill of pattern correlations.

References

- Adler RF, Huffman GJ, Chang A, Ferraro R, Xie P, Janowiak J, Rudolf B, Schneider U, Curtis S, Bolvin D, Gruber A, Susskind J, Arkin P, Nelkin E (2003) The version-2 global precipitation climatology project (GPCP) monthly precipitation analysis (1979–present). *J Hydrometeorol* 4:1147–1167
- Alessandri A, Borrelli A, Masina S, Carril AF, Di Pietro P, Carril AF, Cherchi A, Gualdi S, Navarra A (2010) The INGV-CMCC seasonal prediction system: improved Ocean initial conditions. *Mon Weather Rev* 138(7):2930–2952
- Alessandri A, Borrelli A, Navarra A, Arribas A, Déqué M, Rogel P, Weisheimer A (2011) Evaluation of probabilistic quality and value of the ENSEMBLES multi-model seasonal forecasts: comparison with DEMETER. *Mon Weather Rev* 139(2):581–607
- An SI (2004) Interdecadal changes in the El Niño-La Nina asymmetry. *Geophys Res Lett* 31:L23210
- An SI, Wang B (2000) Interdecadal change of the structure of ENSO mode and its impact on the ENSO frequency. *J Clim* 13:2044–2055
- Ashok K, Nakamura H, Yamagata T (2007) Impacts of ENSO and IOD events on the Southern Hemisphere storm track activity during austral winter. *J Clim* 20:3147–3163
- Ashok K, Tam CY, Lee WJ (2009) ENSO Modoki impact on the Southern Hemisphere storm track activity during extended austral winter. *Geophys Res Lett* 36:L12705. doi:10.1029/2009GL038847
- Balmaseda MA, Vidard A, Anderson D (2008) The ECMWF ORA-S3 ocean analysis system. *Mon Weather Rev* 136(3):18–34
- Behringer DW, Xue Y (2004) Evaluation of the global ocean data assimilation system at NCEP: The Pacific Ocean. Eighth symposium on integrated observing and assimilation systems for atmosphere, Oceans, and Land Surface. AMS 84th annual meeting, Washington State Convention and Trade Center, Seattle, Washington, pp 11–15
- Cai W, Cowan T (2009) La Niña Modoki impacts Australia autumn rainfall variability. *Geophys Res Lett* 36:L12805. doi:10.1029/2009GL037885
- Chen M, Xie P, Janowiak JE, Arkin PA (2002) Global land precipitation: a 50-yr monthly analysis based on gauge observations. *J Hydrometeorol* 3:249–266
- Collins WJ, Bellouin N, Doutriaux-Boucher M, Gedney N, Hinton T, Jones CD, Liddicoat S, Martin G, O'Connor F, Rae J, Senior C,

- Totterdell I, Woodward S, Reichler T, Kim J, Halloran P (2008) Evaluation of the HadGEM2 model. Hadley Centre Technical Note HCTN 74, Met Office Hadley Centre, Exeter, UK. <http://www.metoffice.gov.uk/learning/library/publications/science/climate-science>
- Daget N, Weaver AT, Balmaseda MA (2009) Ensemble estimation of background-error variances in a three-dimensional variational data assimilation system for the global ocean. *Q J R Meteorol Soc* 135:1071–1094
- Diaz HF, Hoerling MP, Eischeid JK (2001) ENSO variability, teleconnections and climate change. *Int J Climatol* 21:1845–1862
- Graham NE (1992) Decadal scale climate variability in the 1970s and 1980s: observations and model results: decadal-to-century time scales of climate variability. Academic, New York
- Graham NE (1994) Decadal scale variability in the tropical and North Pacific during the 1970s and 1980s: observations and model results. *Clim Dyn* 10:135–162
- Gu D, Philander S (1997) Interdecadal climate fluctuations that depend on exchanges between the tropics and extratropics. *Science* 275:805–807
- Guilyardi E, Bellenger H, Collins M, Ferrett S, Cai W, Wittenberg A (2012) A first look at ENSO in CMIP5. *CLIVAR Exch* 17:29–32
- Hare SR, Mantua NJ (2000) Empirical evidence for North Pacific regime shifts in 1977 and 1989. *Prog Oceanogr* 47:103–145
- Hendon HH, Lim E, Wang G, Alves O, Hudson D (2009) Prospects for predicting two flavors of El Niño. *Geophys Res Lett* 36:L19713. doi:10.1029/2009GL040100
- Hollowed AB, Hare SR, Wooster WS (2001) Pacific basin climate variability and patterns of northeast Pacific marine fish production. *Prog Oceanogr* 49:257–282
- Jeong HI, Lee DY, Ashok K, Ahn JB, Lee JY, Luo JJ, Schemm JK, Hendon HH, Braganza K, Ham YG (2012) Assessment of the APCC coupled MME suite in predicting the distinctive climate impacts of two flavors of ENSO during boreal winter. *Clim Dyn* 39:475–493
- Jia XJ, Lin H, Lee JY, Wang B (2012) Season-dependent forecast skill of the leading forced atmospheric circulation pattern over the North Pacific and North American Region. *J Clim* 25:7248–7265
- Jia XJ, Lee JY, Lin H (2014) Interdecadal change in the Northern Hemisphere seasonal climate prediction: Part I. The leading forced mode of atmospheric circulation. *Clim Dyn*. doi:10.1007/s00382-013-1988-1
- Jin EK, Kinter JL III, Wang B, Park CK, Kang IS, Kirtman BP, Kug JS, Kumar A, Luo JJ, Schemm J, Shukla J, Yamagata T (2008) Current status of ENSO prediction skill in coupled O-A models. *Clim Dyn* 31:647–664. doi:10.1007/s00382-008-0397-3
- Kalnay E, Kanamitsu M, Kistler R, Collins W, Deaven D, Gandin L, Iredell M, Saha S, White G, Woollen J, Zhu Y, Chelliah M, Ebisuzaki W, Higgins W, Janowiak J, Mo KC, Ropelewski C, Wang J, Leetma A, Reynolds R, Jenne R, Joseph D (1996) The NCEP/NCAR 40-year reanalysis project. *Bull Am Meteorol Soc* 77:437–471
- Kang H, Park CK, Saji NH, Ashko K (2009) Statistical downscaling of precipitation in Korea using multimodel output variables as predictors. *Mon Weather Rev* 137:1928–1938
- Kao HY, Yu JY (2009) Contrasting eastern-Pacific and central-Pacific types of ENSO. *J Clim* 22:615–632
- Keenlyside N, Latif M, Botzet M, Jungclauss J, Schulzweida U (2005) A coupled method for initializing el niño southern oscillation forecasts using sea surface temperature. *Tellus A* 57:340–356
- Kim ST, Yu JY (2012) The two types of ENSO in CMIP5 models. *Geophys Res Lett* 39:L11704. doi:10.1029/2012GL052006
- Kim JS, Kim KY, Yeh SW (2012) Statistical evidence for the natural variation of the central Pacific El Niño. *J Geophys Res* 117:C06014. doi:10.1029/2012JC008003
- Kodera K (2010) Change in the ENSO teleconnection characteristics in the boreal winter. *SOLA* 6A:21–24
- Kug JS, Jin FF, An SI (2009) Two types of El Niño events: cold tongue El Niño and warm pool El Niño. *J Clim* 22:1499–1515
- Larkin NK, Harrison DE (2005) Global seasonal temperature and precipitation anomalies during El Niño autumn and winter. *Geophys Res Lett* 32:L16705. doi:10.1029/2005GL022860
- Lee T, McPhaden MJ (2010) Increasing intensity of El Niño in the central-equatorial Pacific. *Geophys Res Lett* 37:L14603. doi:10.1029/2010GL044007
- Lee JY, Wang B (2014) Future change of global monsoon in the CMIP5. *Clim Dyn* 42:101–119. doi:10.1007/s00382-012-1564-0
- Lee DY, Tam CY, Park CK (2008) Effects of multicumulus convective ensemble on East Asian summer monsoon rainfall simulation. *J Geophys Res* 113:D24111. doi:10.1029/2008JD009847
- Lee JY, Wang B, Kang IS, Shukla J, Kumar A, Kug JS, Schemm JKE, Juo JJ, Yamagata T, Fu X, Alves O, Stern B, Rosati T, Park CK (2010) How are seasonal prediction skills related to models performance on mean state and annual cycle? *Clim Dyn* 35:267–283
- Lee DY, Ashok K, Ahn JB (2011a) Toward enhancement of prediction skills of multimodel ensemble seasonal prediction: a climate filter concept. *J Geophys Res* 116:D06116. doi:10.1029/2010JD014610
- Lee JY, Wang B, Ding Q, Ha KJ, Ahn JB, Kumar A, Stern B, Alves O (2011b) How predictable is the NH summer upper-tropospheric circulation? *Clim Dyn* 37:1189–1203
- Lee SS, Lee JY, Ha KJ, Wang B, Schemm JK (2011c) Deficiencies and possibilities for long-lead coupled climate prediction of the western North Pacific-East Asian summer monsoon. *Clim Dyn* 36:1173–1188
- Lee JY, Lee SS, Wang B, Ha KJ, Jhun JG (2013) Seasonal prediction and predictability of the Asian winter temperature variability. *Clim Dyn* 41:573–587
- Lee JY, Wang B, Seo KH, Kug JS, Choi YS, Kosaka Y, Ha KJ (2014) Future change of Northern Hemisphere summer tropical-extra-tropical teleconnection in CMIP5 models. *J Clim*. doi:10.1175/JCLI-D-13-00261.1
- Lim EP, Hendon HH, Hudson D, Wang G, Alves O (2009) Dynamical forecast of inter-El Niño variations of tropical SST and Australian spring rainfall. *Mon Weather Rev* 137:3796–3810
- Lim EP, Hendon HH, Langford S, Alves O (2012) Improvements in POAMA2 for the prediction of major climate drivers and south eastern Australian rainfall. CAWCR Tech. Rep. No. 051. <http://www.cawcr.gov.au/publications/technicalreports.php>
- Maslanik JA, Serreze MC, Barry RG (1996) Recent decreases in Arctic summer ice cover and linkages to atmospheric circulation anomalies. *Geophys Res Lett* 23:1677–1680
- McPhaden MJ, Lee T, McClurg D (2011) El Niño and its relationship to changing background conditions in the tropical Pacific Ocean. *Geophys Res Lett* 38:L15709. doi:10.1029/2011GL048275
- Nitta T, Yamada S (1989) Recent warming of tropical sea surface temperature and its relationship to the Northern Hemisphere circulation. *J Meteorol Soc Jpn* 67:375–383
- Overland JE, Wang M (2005) The Arctic climate paradox: the recent decrease of the Arctic Oscillation. *Geophys Res Lett* 32:L06701. doi:10.1029/2004GL021752
- Peng P, Kumar A, Van den Dool HM, Barnston AG (2002) An analysis of multimodel ensemble predictions for seasonal climate anomalies. *J Geophys Res* 107(D23):4710. doi:10.1029/2002JD002712
- Ropelewski CF, Halpert MS (1987) Global and regional scale precipitation patterns associated with the El Niño/Southern Oscillation. *Mon Weather Rev* 115:1606–1626

- Ropelewski CF, Halpert MS (1989) Precipitation patterns associated with the high index phase of the Southern Oscillation. *J Clim* 2:268–284
- Saji NH, Yamagata T (2003) Possible impacts of Indian Ocean dipole mode events on global climate. *Clim Res* 25:151–169
- Salas-Méllia D (2002) A global coupled sea ice-ocean model. *Ocean Model* 4:137–172
- Shi L, Hendon H, Alves O, Luo JJ, Balmaseda M, Anderson D (2012) How predictable is the Indian Ocean Dipole? *Mon Weather Rev* 140:3867–3884
- Shinoda T, Hendon HH, Alexander MA (2004) Surface and subsurface dipole variability in the Indian Ocean and its relation to ENSO. *Deep-Sea Res* 51:619–635
- Smith TM, Reynolds RW, Peterson TC, Lawrimore J (2008) Improvements to NOAA's historical merged land-ocean surface temperature analysis (1880–2006). *J Clim* 21:2283–2296
- Stevenson S, Fox-Kemper B, Jochum M, Neale R, Deser C, Meehl G (2012) Will there be a significant change to El Niño in the 21st century? *J Clim* 25:2129–2145
- Stockdale TN, Anderson DLT, Balmaseda MA, Doblas-Reyes FJ, Ferranti L, Mogensen K, Palmer TN, Molteni F, Vitart F (2011) ECMWF seasonal forecast system 3 and its prediction of sea surface temperature. *Clim Dyn* 37:455–471
- Tang Y, Deng Z, Zhou X, Chen Y (2008) Interdecadal variation of ENSO predictability in multiple models. *J Clim* 21:4811–4833
- Taschetto AS, England MH (2009) El Niño Modoki impacts on Australian rainfall. *J Clim* 22:3167–3174. doi:[10.1175/2008JCLI2589.1](https://doi.org/10.1175/2008JCLI2589.1)
- Trenberth K, Hurrell J (1994) Decadal atmosphere-ocean variations in the Pacific. *Clim Dyn* 9:303–319
- Wallace JM, Gutzler DS (1981) Teleconnections in the potential height field during the Northern Hemisphere winter. *Mon Weather Rev* 109:784–812. doi:[10.1175/1520-0493](https://doi.org/10.1175/1520-0493)
- Wallace JM, Rasmusson EM, Mitchell TP, Kousky VE, Sarachik ES, Storch H (1998) The structure and evolution of ENSO-related climate variability in the tropical Pacific: lessons from TOGA. *J Geophys Res* 103(14):241–259
- Walsh JE, Chapman WL, Shy TL (1996) Recent decrease of sea level pressure in the central Arctic. *J Clim* 9:480–486
- Wang G, Hendon HH (2007) Sensitivity of Australian rainfall to inter-El Niño variations. *J Clim* 20:4211–4226
- Wang B, Wang Y (1996) Temporal structure of the Southern Oscillation as revealed by waveform and wavelet analysis. *J Clim* 9:1586–1598
- Wang B, Lee JY, Kang IS, Shukla J, Kug JS, Kumar A, Schemm J, Luo JJ, Yamagata T, Park CK (2008a) How accurately do coupled climate models predict the leading modes of Asian-Australian monsoon interannual variability? *Clim Dyn* 30:605–619
- Wang B, Yang J, Zhou T (2008b) Interdecadal changes in the major modes of Asian-Australian monsoon variability: strengthening relationship with ENSO since the late 1970s. *J Clim* 21:1771–1789
- Wang B, Lee JY, Kang IS, Shukla J, Park CK, Kumar A, Schemm J, Cocks S, Kug JS, Luo JJ, Zhou T, Wang B, Fu X, Yun WT, Alves O, Jin EK, Kinter J, Kirtman B, Krishnamurti T, Lau NC, Lau W, Liu P, Pegion P, Rosati T, Schubert S, Stern W, Suarez M, Yamagata T (2009) Advance and prospectus of seasonal prediction: assessment of the APCC/CLIPAS 14-model ensemble retrospective seasonal prediction (1980–2004). *Clim Dyn* 33:93–117
- Watanabe M, Nitta T (1999) Decadal changes in the atmospheric circulation and associated surface climate variations in the Northern Hemisphere winter. *J Clim* 12:494–510
- Weisheimer A, Doblas-Reyes FJ, Palmer TN, Alessandri A, Arribas A, Déqué M, Keenlyside N, MacVean M, Navarra A, Rogel P (2009) Ensembles: a new multi-model ensemble for seasonal-to-annual predictions-skill and progress beyond Demeter in forecasting tropical Pacific SSTs. *Geo Res Lett* 36:L21711
- Weng H, Ashok K, Behera SK, Rao SA, Yamagata T (2007) Impacts of recent El Niño Modoki on dry/wet conditions in the Pacific rim during boreal summer. *Clim Dyn* 29:113–129
- Weng H, Behera SK, Yamagata T (2009) Anomalous winter climate conditions in the Pacific rim during recent El Niño Modoki and El Niño events. *Clim Dyn* 32:663–674
- Wu A, Hsieh W (2003) Nonlinear interdecadal changes of the El Niño-southern oscillation. *Clim Dyn* 21:719–730
- Yasunaka S, Hanawa K (2003) Regime shifts in the Northern Hemisphere SST field: revisited in relation to tropical variations. *J Meteorol Soc Jpn* 81:415–424
- Yeh SW, Kug JS, Dewitte B, Kwon MH, Kirtman BP, Jin FF (2009) El Niño in a changing climate. *Nature* 461:511–514
- Yeh SW, Kirtman BP, Kug JS, Park W, Latif M (2011a) Natural variability of the central Pacific El Niño event on multicentennial timescales. *Geophys Res Lett* 38:L02704. doi:[10.1029/2010GL045886](https://doi.org/10.1029/2010GL045886)
- Yeh SW, Kang Y, Noh Y, Miller A (2011b) The North Pacific climate transitions of the winters of 1976/77 and 1988/89. *J Clim* 24:1170–1183
- Yu JY, Kao HK (2007) Decadal changes of ENSO persistence barrier in SST and ocean heat content indices: 1958–2001. *J Geophys Res* 112:D13106. doi:[10.1029/2006JD007654](https://doi.org/10.1029/2006JD007654)
- Yu JY, Lu MM, Kim ST (2012a) A change in the relationship between tropical central Pacific SST variability and the extratropical atmosphere around 1990. *Environ Res Lett* 7. doi:[10.1088/1748-9326/7/3/034025](https://doi.org/10.1088/1748-9326/7/3/034025)
- Yu JY, Zou Y, Kim ST, Lee T (2012b) The changing impact of El Niño on US winter temperatures. *Geophys Res Lett* 39:L15702